Flux-flow noise in type-II superconductors

W. J. Yeh
Department of Physics, University of Idaho, Moscow, Idaho 83843

Y. H. Kao
Department of Physics, State University of New York at Buffalo, Buffalo, New York 14260
(Received 27 July 1990; revised manuscript received 26 December 1990)

Measurements of flux flow in type-II superconductors by a direct flux-detection method are described. A superconducting-quantum-interference-device magnetometer is employed to monitor the fluctuating component of flux changes in the central part of $In_{0.9}Pb_{0.1}$ alloy samples as a function of the transport current. Experimental results show that the behavior of flux flow in the high-current region is significantly different from that near the onset. For high-current values, the noise-power spectral density can be fitted quite well by a Lorentzian form, and the rolloff frequency varies linearly with the current as well as the length, but not the width, of the detection loop. A simple model is proposed to account for these observations. The number of moving bundles is estimated from the data, and its low value suggests that only a small fraction of flux lines form sizable bundles that can be detected in this experiment. In the near-onset region, the average ac output of the detector shows several distinct peaks as the transport current is increased. Power spectra exhibit the form of $1/f$ noise at the peak positions, whereas deviations from $1/f$ noise are found at positions away from the peaks. The $1/f$ noise as well as deviations from $1/f$ can be explained by assuming a velocity spread of the moving bundles.

I. INTRODUCTION

It is well known that magnetic fluxoids in type-II superconductors can be driven into motion by applying a dc transport current in the sample perpendicular to the magnetic field. It follows that a time-averaged dc voltage as well as a fluctuating ac voltage can be generated in the sample. The dynamical properties of this flux motion have been extensively studied in the past.[1,2] Of special interest is the study of the ac component (or flux-flow noise), initiated by van Ooijen and van Gurp,[3] from which specific information about the dynamical behavior of the fluxoid motion can be derived.

In essence, van Ooijen and van Gurp[3] used a shot-noise model to explain their experimental results obtained with potential probes attached to the specimen. An individual flux entity Φ (either a singly quantized flux line or a bundle of flux tubes) that moves across the sample with a transit time τ will give rise to a rectangular voltage pulse with height Φ/τ and width τ. If the flux bundles are of the same size and move independently in a random fashion with the same velocity, in accordance with a shot-noise theory,[4] this process will result in a noise-power spectrum of the form $2\Phi V(\sin p/p)^2$, where $p=\pi f\tau$, with a rolloff frequency $f_c=1/\tau=v/W$, where V is the time-averaged dc voltage, v is the velocity of flux lines, and W is the width of the sample. A number of experimental and theoretical investigations[5-27] were reported after the work of van Ooijen and van Gurp. These studies, however, have not yet led to a consistent description of the dynamical processes of flux motion in superconductors.

A chain model was proposed by Chilton[5] and later extended by Wade.[6] They suggested that flux motion might take the form of vortices moving in columns (or chains of vortices) extending form one side of the sample to the other. The neighboring chains are uncorrelated, and the flux lines between chains are stationary. This model was also used by Jarvis and Park[7] to account for the extremely small bundle size deduced from their data.

Another model used by Jarvis and Park[8] and Joiner and co-workers[9,10] assumes that the flux motion is interrupted by pinning centers, so that the voltage pulses originally proposed by van Ooijen and van Gurp[3] are divided into subpulses. By an appropriate choice of the range of the subpulse widths, their data can be fitted very well by this model.

Flux-flow noise and correlation functions were extensively studied by Heiden and co-workers.[11-18] For samples containing many small grains, their results seem to support an assumption that the flux-flow noise is due to locally generated random fluctuations of vortex velocity and density caused by the pinning centers. These fluctuations can lead to distortions of the otherwise homogeneous arrangement of vortices which travel with an average velocity v. In view of their results, it seems that the model of van Ooijen and van Gurp may be applied to samples only with very large grain sizes.[13,15]

Burgess[19] and Clem[20-23] have calculated power spectra of flux-flow noise. In particular, Clem predicted that the spectra should depend on the ratio of the separation between voltage probes to the width of the sample.[20] This prediction, however, has not been completely verified by experiment.[7]

In view of the different results reported in various experimental studies and discrepancies between theoretical

 ©1991 The American Physical Society

predictions and experiments, it seems desirable to investigate the flux motion by using a new independent method. This is the motivation of the present work. The superconducting quantum interference device (SQUID) is a natural candidate for this measurement because of its extremely high sensitivity to changes of magnetic flux. Under proper shielding conditions, it can be arranged to respond mainly to the flux changes in its input detection loop closely coupled to the superconducting sample. Some results of such an experiment have been reported before.[28] Recently, Ferrari *et al.*[29] also used a SQUID to measure flux noise in high-temperature superconducting thin films under zero-bias current. In the present paper, we describe more detailed measurements of flux-flow noise in conventional type-II superconductors by using a SQUID to monitor directly the fluctuating component of flux flow. The rest of the paper is organized as follows. In Sec. II the experimental details and sample preparation are described. The main experimental results are given in Sec. III. Because of quite different behavior observed in the experiments, the total flux-flow regime is divided into a "near-onset region" and a "quasilinear region." In Sec. IV a model for flux-flow noise in the quasilinear region is developed. Section V discusses bundle size, number of observed flux bundles, $1/f$ noise, and flicker noise. The last section presents our conclusion, and the relevance of our method to the investigation of high-T_c superconductors is pointed out.

II. EXPERIMENT

A. Preparation and mounting of samples

Samples used in this experiment are sheets of indium (90%) and lead (10%) alloy. The κ value of the material at the temperatures of our measurements[30] is around 1.5. The pure material obtained from A.D. Mackay Company was melted in a vacuum of 1×10^{-6} Torr in a molybdenum boat coated with Al_2O_3. After the material was melted and cooled down, the ingot was flattened by a rolling machine. The direction of rolling was frequently changed so as to avoid a preferred direction in the stretch. After the thickness reached the required value (50 μm), the sample was cut by razor blades to the desired shape. The dimensions of samples were approximately $2\times12\times0.005\text{mm}^3$, with two attached terminals 8 mm apart along the length direction for voltage measurements. Most of the samples were annealed at 130 °C in air for 6 h. Only the sample 7 was not annealed, but it had stayed in air for 4 months before it was used.

The sample was affixed to clean sapphire substrate by GE varnish. A small rectangular detection loop made of thin insulated niobium wire (0.003-in. diameter) was placed on the surface of the sample; the longer side of the rectangular loop was parallel to the direction of the transport current. The rest of the detection coil was shielded by a thin lead tubing. The ends of the detection coil were connected to the input terminals of an rf SQUID which monitored the flux change in the detection loop. Pertinent information about the samples and detection loops is given in Table I. The $H_{c2}(0)$ values were obtained from $H_{c2}(T)=H_{c2}(0)[1-(T/T_c)^2]$ by measuring $H_{c2}(T)$ at several low temperatures (where κ is nearly constant). It should be noted that in our experiment the temperature was in the range from 2.9 to 4.2 K, and the magnetic field was between 150 and 500 Oe. We always maintained the magnetic field higher than H_{c1} of the sample. However, this field was much lower than the H_{c1} of niobium within the temperature range of the experiment, so that the magnetic flux could not penetrate into the niobium wires. This condition was essential in order to avoid spurious effects arising from flux flow in the niobium detection loop.

The sample was mounted on a holder which was placed between two superconducting Helmholtz coils in the direction that the magnetic field was perpendicular to the broad face of the sample. The Helmholtz coils were operated in superconducting persistent mode in order to maintain a stable magnetic field. The entire assembly was shielded from ambient magnetic field by a long lead superconducting cylinder with a closed bottom. The helium Dewar was magnetically shielded by two concentric μ-metal layers, which reduced the residual magnetic field to a level of about 10^{-3} Oe. The measurements were made in a screened room.

TABLE I. Some properties of samples and detection loops.

Sample	Critical temperature T_c (K)	Critical magnetic field $H_{c2}(0)$ (Oe)	Sample dimensions w (mm)	l (mm)	t(mm)	Detection loop dimensions W (mm)	L (mm)	Treatment condition	Ginzburg-Landau parameter κ	Lead atomic percent
1	4.41	1270	1.35	7.5	0.05	0.2	4	annealed at 130 °C for 6 h	1.5	10
2	4.34	1207	1.8	8.7	0.05	0.2	4	same as above	1.5	10
3	4.34	1207	1.95	6.6	0.05	0.2	1.6	same as above	1.5	10
4	4.42	1237	1.9	8.0	0.05	0.2	4	same as above	1.5	10
5	4.37	1140	2.6	8.7	0.05	1	4	same as above	1.5	10
6	4.37	1140	2.15	8.0	0.05	0.6	2	same as above	1.5	10
7	4.42	1247	1.8	8.1	0.05	0.2	4	unannealed	1.5	10

B. Measurement circuit

A schematic diagram for the whole system is shown in Fig. 1. The section enclosed within the dotted line was in low temperature. The dc current for the sample was supplied by a stable dc power supply, and the dc voltage V induced by flux motion was measured with a Keithley 148 nanovoltmeter.

When the flux lines under the detection loop were in motion, the time-dependent output of the rf SQUID can be written as

$$V_R(t)=\langle V_R \rangle+\delta V_R(t) , \quad (1)$$

where $\langle V_R \rangle$ is the time-averaged output of the SQUID and $\delta V_R(t)$ is the ac component of the output. The part $\langle V_R \rangle$ includes two contributions. The major effect comes from the average flux changes in the total flux lies in the detection loop, and a small amount of flux lines generated by the driving current will also link through the detection loop, giving rise to a small contribution. The latter part depends on the relative positions of the loop and the sample as well as the smoothness of the sample. Because the latter condition cannot be accurately controlled, $\langle V_R \rangle$ cannot be considered reliably as a useful measure of the flux motion. Therefore, $\langle V_R \rangle$ was not recorded in most cases. The output terminals of the rf SQUID could be connected to an oscilloscope to see the variation of $\delta V_R(t)$, to a spectrum analyzer to measure the power spectral density distribution of $\delta V_R(t)$, or to a lock-in amplifier used as an ac voltmeter to measure its rms amplitude. The last quantity will be represented by $\langle \delta V_R \rangle$ in the text. When this lock-in amplifier is used as an ac voltmeter, the meter reading is within 12% of the wideband rms amplitude of the signal, and its bandwidth of frequency response is from 0.1 Hz to 0.1 MHz. This wide bandwidth covers the range of frequency response of the rf SQUID used in our experiment.

The rf SQUID was in most cases operated in the "fast" mode with no filter applied. The bandwidth of this SQUID in this condition is from dc to 20 kHz. For small signals, high-frequency information (up to 210 kHz) could also be obtained from the HF (high-frequency) output. A small tightly wound solenoid was used as a known flux source to calibrate the detection system; the result was that a change of single flux quantum in the detection loop corresponds to an output amplitude of 2.2 mV with the "$\times 10$" setting used in our experiment. The lowest temperature at which the SQUID can function was approximately 2.9 K; hence all of our experiments were performed at temperatures higher than the λ point of liquid helium.

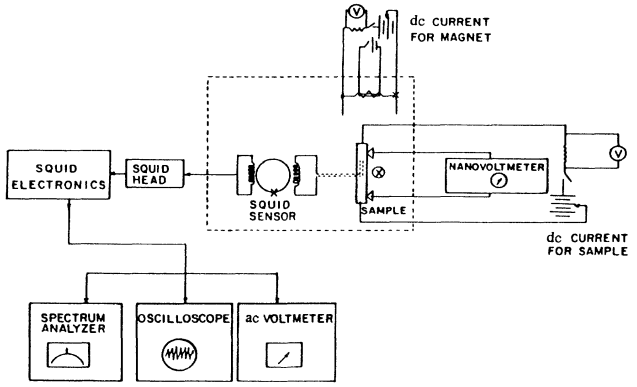

FIG. 1. Experimental setup for flux-flow noise measurements.

III. EXPERIMENTAL RESULTS

All of our experimental results were obtained from three types of measurements, namely, the dc voltage versus transport current (V-versus-I curves), the amplitude of $\delta V_R(t)$ versus transport current ($\langle \delta V_R \rangle$-versus-$I$ curves), and the power spectra of $\delta V_R(t)$.

A. V-versus-I curves

A typical set of V-versus-I curves at different magnetic fields is shown in Fig. 2. The data were obtained with the sample 6 at $T=3.672$ K. The general features of the V-versus-I curves are as follows: The voltage remains zero until the current reaches a critical value. As the current passes the critical value, the voltage begins to appear and increases nonlinearly in a region near the voltage onset. This is called the "near-onset region" of flux flow. The reason for this strongly nonlinear behavior is mainly due to pinning effects. As the current is increased further, the relationship between the current and voltage becomes nearly linear and is called the "quasilinear region." It should be noted that the V-I curves in this region are al-

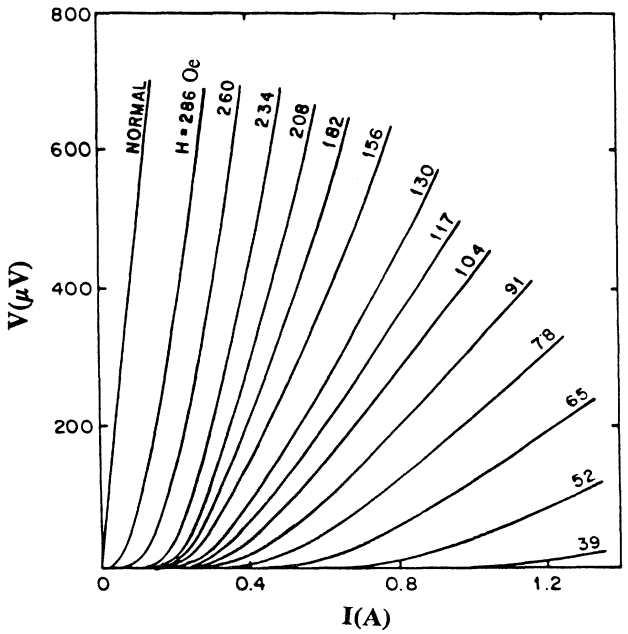

FIG. 2. Typical set of V-vs-I curves obtained with sample 6 at $T=3.672$ K in different magnetic fields.

ways concave upward, indicating a nonconstant dynamical resistance. The nonlinearity of the V-I curve at relatively high currents could be partly due to self-heating. The flicker noise which results from this effect will be discussed in Sec. V.

B. $\langle \delta V_R \rangle$-versus-$I$ curves

Useful information and some new features of flux flow were revealed from measurements of the ac voltage of the SQUID output δV_R. There are generally two ways in which these measurements were made. First, the real shape of the noise voltage $\delta V_R(t)$ can be directly viewed from an oscilloscope. Figures 3(b) and 3(c) are typical oscilloscope pictures taken in the near-onset and quasilinear region, respectively. These pictures show basic difference between the noise $\delta V_R(t)$ in these two regions. In the near-onset region, the individual $\delta V_R(t)$ voltage jumps show strong overlap, giving rise to a large amplitude fluctuation. In the quasilinear region, the $\delta V_R(t)$ signal shows less amplitude variation (note the change in scale). In the second method the average amplitude of the ac signal ($\langle \delta V_R \rangle$) was measured directly by using an ac voltmeter across the output terminals of the SQUID. Because the ac signal observed by the first method cannot be recorded in a continuous manner when I is varied, we have used the second method to take data of $\langle \delta V_R \rangle$. Its calibration, however, was done by using the first method.

Figure 4(a) is a typical set of $\langle \delta V_R \rangle$-versus-$I$ curves with the applied magnetic field as a parameter. Figure 4(b) is an enlargement of the $\langle \delta V_R \rangle$-versus-$I$ curve with $H = 227.5$ Oe taken at a later time. These data were taken with the sample 2 at $T = 3.672$ K. For the sake of comparison, in Fig. 4(b) and V-versus-I curve under the same condition was also recorded, and the dc voltage in the specimen was measured with a nanovoltmeter connected to the two attached leads. Unlike the smooth variation of V with I, $\langle \delta V_R \rangle$ exhibits complex structures

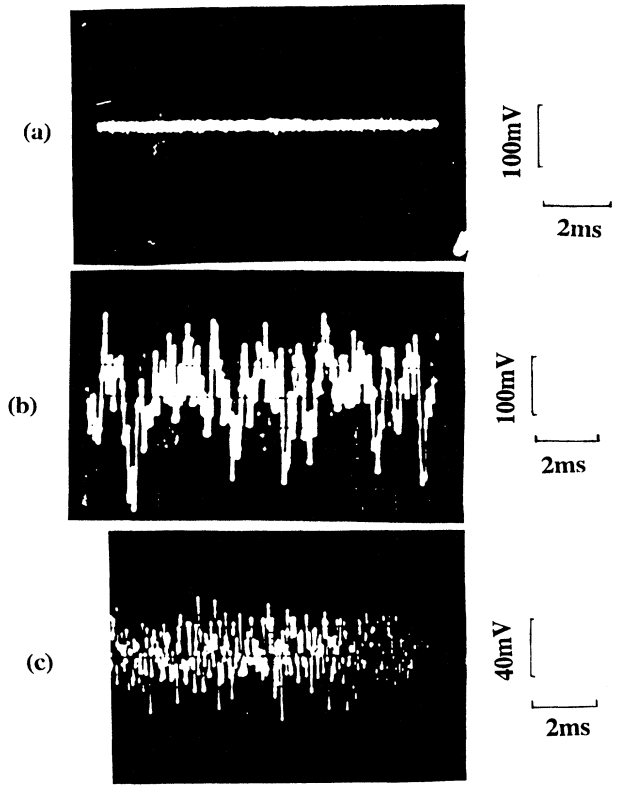

FIG. 3. Typical oscilloscope traces showing (a) intrinsic noise of the rf SQUID at the standard output (×10 range, no filter, and in "fast mode"); (b) voltage variation $\delta V_R(t)$ at the onset of flux flow obtained with sample 5 at $T = 4.1$ K, $H = 26$ Oe, and $I = 0.286$ A; (c) voltage variation in the quasilinear region obtained with sample 2 at $T = 3.447$ K, $H = 260$ Oe, and $I = 0.48$ A.

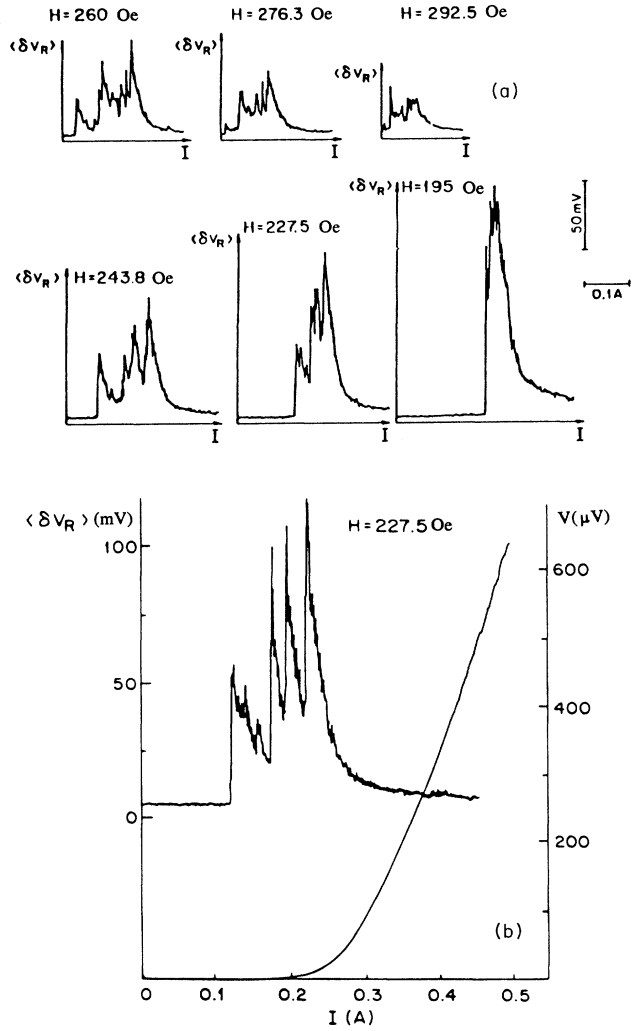

FIG. 4. (a) Typical set of $\langle \delta V_R \rangle$-vs-$I$ curves at different magnetic fields obtained with sample 2 at $T = 3.672$ K. (b) Enlarged plot for the curve in (a) with $H = 227.5$ Oe and the corresponding V-vs-I curve.

in the near-onset region. When the current was increased from zero, $\langle \delta V_R \rangle$ remains at a very low value (it corresponds to the intrinsic noise of the SQUID) until the current reaches the critical current I_0. At I_0, $\langle \delta V_R \rangle$ jumps abruptly to a large value and exhibits several distinct peaks for a certain range of current. As the current is increased further, $\langle \delta V_R \rangle$ decreases rapidly in a short range of current. After that, $\langle \delta V_R \rangle$ decreases slowly and the $\langle \delta V_R \rangle$-versus-$I$ curves become smooth at high-current values.

In the near-onset region, one remarkable feature in the $\langle \delta V_R \rangle$-versus-$I$ curves is that there are several distinct peaks. The first peak gives a sharply defined critical current. The position of the peaks is well defined and can be repeated very well from one run to another, although the height of the peaks may differ slightly. The height of peaks decreases as the temperature or magnetic field is increased. The number of peaks may depend on the temperature and magnetic field and may differ from sample to sample; the relative height of the peaks is also sensitive to temperature and magnetic field.

In the quasilinear region, $\langle \delta V_R \rangle$ decreases gradually with increasing I and the $\langle \delta V_R \rangle$-versus-$I$ curve appears smooth. The value of $\langle \delta V_R \rangle$ in the quasilinear region is much smaller than that in the near-onset region.

The abrupt jump of $\langle \delta V_R \rangle$ at the critical current clearly separates the system into different states, the stationary and flux-flow states. It defines an unambiguous critical current. In previous work the critical current was usually defined by the onset of voltage in the V-versus-I curve. But in the onset region, the voltage is very small and increases gradually with current; detection of this small voltage and determination of the critical current are subject to large errors. It can be seen from Fig. 4(b) that the critical current is not well defined in the V-I curve. From the clean-cut jump of $\langle \delta V_R \rangle$ at the critical current, one can see the great improvement in sensitivity offered by the combination of a SQUID and a voltmeter. The critical current I_0 or critical density J_0 used in this paper were all determined this way.

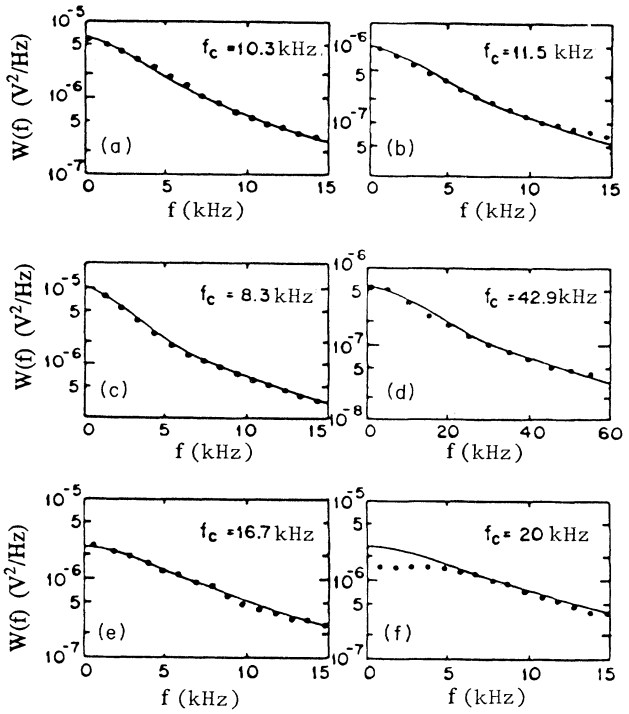

FIG. 5. Set of power spectra in the quasilinear region obtained with various samples at different temperatures, magnetic fields, and current densities. Dots are data points, and solid curves represent best fits to the data by the form $A[1+(\pi f/f_c)^2]^{-1}$; f_c is obtained from the best fit. (a) Sample 1, $T=2.99$ K, $H=325$ Oe, and $I=0.53$ A. (b) Sample 6, $T=3.86$ K, $H=78$ Oe, and $I=0.4$ A. (c) Sample 2, $T=3.447$ K, $H=227.5$ Oe, and $I=0.46$ A. (d) Sample 2, $T=3.447$ K, $H=227.5$ Oe, and $I=0.7$ A. (e) Sample 7, $T=3.447$ K, $H=159.3$ Oe, and $I=0.6$ A. (f) Sample 2, $T=3.86$ K, $H=91$ Oe, and $I=0.4$ A. The detection loop dimensions for (b) are $1\times4\text{mm}^2$; all others are $0.2\times4\text{mm}^2$.

C. Power-spectra measurements

The power spectrum is a very important quantity in the study of flux-flow noise. Some dynamical features of flux flow can be extracted from the power-spectrum measurement. Our experimental results have shown that power spectra in the near-onset region are quite different from those in the quasilinear region. For convenience, power spectra in the quasilinear region will be illustrated first.

1. Power spectra in the quasilinear region

When the system is in the quasilinear region, the power spectra rf SQUID output are well fitted by a Lorentzian expression $A[1+(\pi f/f_c)^2]^{-1}$, where A is a constant and f_c is the characteristic frequency. Several typical power spectral density $W(f)$ curves are shown in Fig. 5. In these figures points are experimental data, solid lines are the best fits to $A[1+(\pi f/f_c)^2]^{-1}$, and f_c in each figure was obtained from the best fit. The detection loop for Fig. 5(b) was $1\times4\text{mm}^2$, and the detection loop for all other figures in this set was $0.2\times4\text{mm}^2$. Power spectra in Figs. 5(c) and 5(d) were taken from the same sample at the same temperature and magnetic field, but with different current densities. Note that the frequency scale in Fig. 5(d) is larger than that of Fig. 5(c). We have accumulated a large number of power spectra at different temperatures, magnetic fields, and current densities with different sizes of detection loops; most of them are well fitted by the Lorentzian expression. A few of them show some low-frequency deviation; Fig. 5(f) is a typical case where the data points fall below the Lorentzian curve in the low-frequency region of the power spectrum. This low-frequency reduction may possibly suggest some long-range correlation in the process, implying that the flux bundles may form a somewhat more regular pattern in some samples.

From Figs. 5(c) and 5(d) it can be seen that when the current density J is increased the characteristic frequency f_c also increases. In order to investigate the relationship

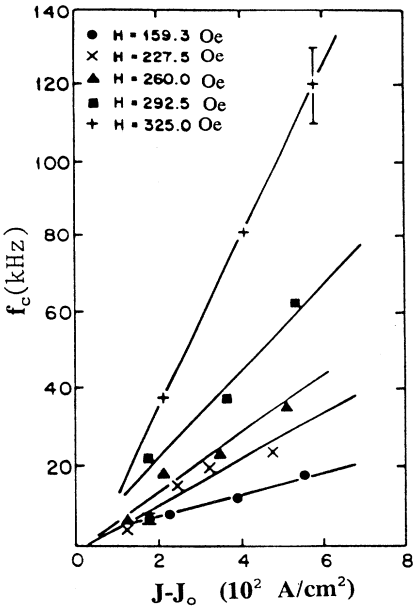

FIG. 6. Plots of f_c vs $(J-J_0)$ obtained with sample 7 at $T=3.447$ K, with magnetic field as a parameter. The solid straight lines represent least-squares fits to the data.

between f_c and J, we plot f_c versus $(J-J_0)$ using temperature and magnetic field as parameters. Figure 6 is a plot of f_c versus $(J-J_0)$ taken from the sample 7 at various magnetic fields, and the temperature was kept constant at 3.447 K. This plot demonstrates a linear relation between f_c and $(J-J_0)$. The straight lines in the plot represent least-squares fits to the data. The slope of the straight line increases as the magnetic field as increased. Figure 7 is a plot of f_c versus $(J-J_0)$ taken from the sample 1 at different temperatures, while the reduced magnetic field h $(=H/H_{c2})$ remains constant at 0.5.

In order to reveal the relationship between the characteristic frequency f_c and the geometry of the detection loop, two sets of measurements were made. In each of these sets we had similar samples and the same external conditions (temperature and magnetic field), with the same shape but different sizes of the detection loop. Plots of f_c versus $(J-J_0)$ for different loops are shown in Figs. 8 and 9. The geometry of the detection loop for each of the measurements is shown in the inset of the figure. In Fig. 8 the length and width of the detection loop for configuration A are both twice as big as those of configuration B. If the shot-noise model[3] were used, the characteristic frequency f_c should depend on the width W of the loop and the velocity v of the flux lines in accordance with $f_c=v/W$; hence the loop with a larger width should lead to a lower characteristic frequency when the velocity remains constant. Since the external conditions for the two configurations were the same, the velocities should be about equal for the same current density. Obviously, our experimental results are inconsistent with the consequence of the shot-noise model.

The effect of the length of the loop on the characteristic frequency can be seen more clearly in Fig. 9(a), in which the width was kept constant while the length was changed. The results show that a shorter length leads to a lower characteristic frequency. Measurements for loops with constant length but different widths show that f_c remains practically unchanged. The difference in f_c shown in Fig. 8 is believed all due to the length variation. The $\langle \delta V_R \rangle$-versus-$I$ curves for configurations B and A in Fig. 9(a) are depicted in Figs. 9(b) and 9(c), respectively. These curves show that the signal amplitudes for both cases are nearly the same in the high-current region, suggesting that the moving flux bundles in these two configurations are of similar size.

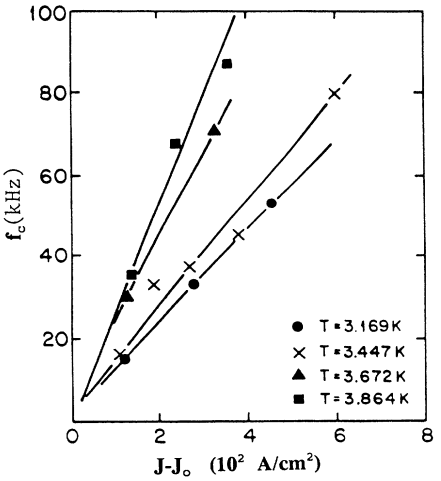

FIG. 7. Plots of f_c vs $(J-J_0)$ obtained with sample 1 at $h=0.5$, with the temperature as a parameter. The solid straight lines represent least-squares fits to the data.

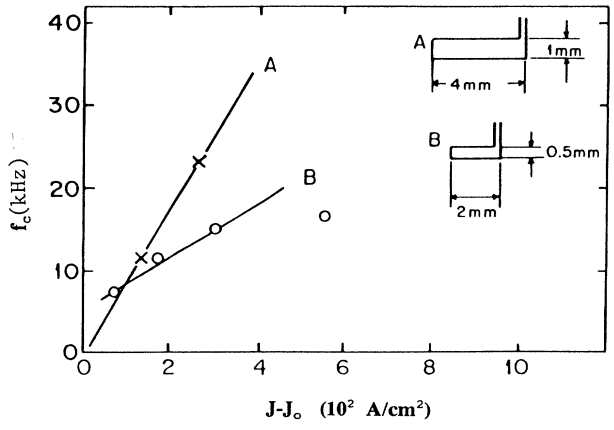

FIG. 8. Plots of f_c vs $(J-J_0)$ obtained with two different detector configurations. All the data were taken at $T=3.86$ K and $H=78.0$ Oe, A for sample 5 and B for sample 6. The configurations of the detection loop are shown in the insets.

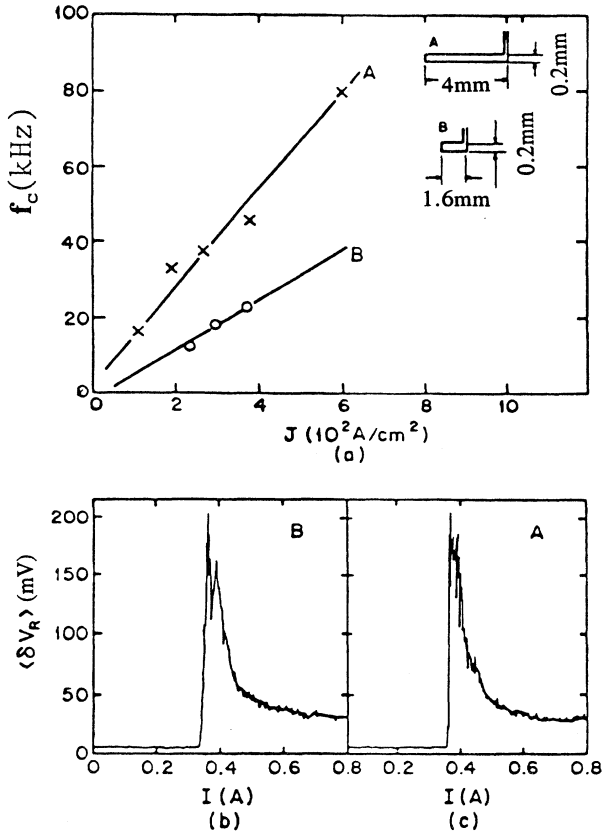

FIG. 9. (a) Plots of f_c vs $(J-J_0)$ obtained with different lengths of the detection loop. All the data were taken at $T=3.447$ K and $H=227.5$ Oe, A for sample 2 and B for sample 3. The configurations of the detection loop are shown in the insets. (b) The $\langle \delta V_R \rangle$-vs-$I$ curve for B. (c) The $\langle \delta V_R \rangle$-vs-$I$ curve for A.

The measurement of f_c with various lengths and widths of the detector loop also lends experimental support to our earlier assumption that the presence of a superconducting Nb detector loop atop the sample has a negligible effect on the observed flux-flow noise. In principle, it may be argued that the Nb wire could present a potential barrier to the motion of fluxons in or out of the detector loop, possibly as a result of local disturbance of field distribution in the immediate neighborhood of the Nb wire or penetration of some fluxons into the Nb wire. Although these possible contributions of the Nb loop are difficult to check quantitatively, our results clearly indicate that the width of the detector loop used in the present experiment was always large enough that f_c actually remained unchanged when the detector width was varied while its length was kept constant. Or the flux-flow phenomena that took place in the sample observed in the present experiment were practically not influenced by the Nb wire. Hence our results, and the interpretations of flux-flow noise henceforth (see Sec. V), are independent of the possible minor perturbation due to the presence of the Nb detector loop.

2. *Power spectra in the near-onset region*

Instead of the Lorentzian shape, the power spectral density can become inversely proportional to frequency in the near-onset region as shown in Fig. 10. All data were taken at the peak positions of the $\langle \delta V_R \rangle$-versus-$I$ curves. The straight lines in the figure are guides for eyes. Because of the frequency limitation of our power-spectrum analyzer, we could not measure power spectral density lower than 200 Hz. In the 200 Hz-to-15 kHz frequency range of our measurements, the slopes of these straight lines are close to -1. Although $1/f$-type noise was observed in some previous flux-flow noise studies,[6,7] no detailed explanation was given. The present experiment shows that different types of power spectra ($1/f$ and Lorentzian types) can be observed in the *same* flux-flow system. This observation also provides some clues for the explanation of the $1/f$ noise in flux motion (see Sec. V).

Deviations from the $1/f$-type distribution were also observed. To illustrate the deviations, a set of power spectra is depicted in Fig. 11(a). This set of data was taken from one sample with fixed temperature and mag-

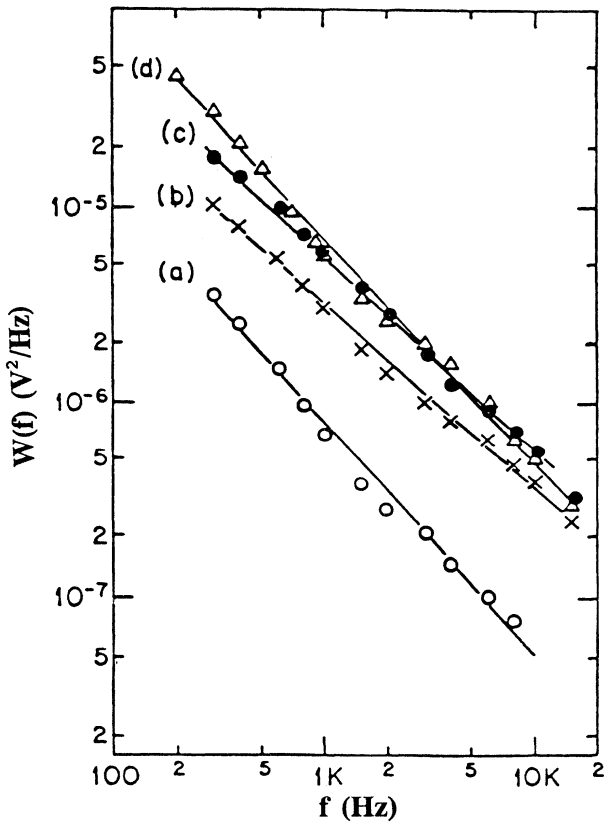

FIG. 10. Power spectra measured in the near-onset region. All the data were taken at $\langle \delta V_R \rangle$ peak positions. (a) Sample 4 at $T=4.03$ K, $H=182$ Oe, and $I=0.018$ A. (b) Sample 4 at $T=4.03$ K, $H=143$ Oe, and $I=0.142$ A. (c) Sample 4 at $T=4.22$ K, $H=52$ Oe, and $I=0.13$ A. (d) Sample 2 at $T=3.45$ K, $H=295$ Oe, and $I=0.395$ A.

netic field, but at different current values. The solid lines in the figure are guides for eyes. Figure 11(b) is the $\langle \delta V_R \rangle$-versus-$I$ curve corresponding to the conditions for Fig. 11(a). The positions indicated by arrows correspond to current values where the power spectra in Fig. 11(a) were taken. The results show that both the shape and amplitude of the power spectrum are very sensitive to current values. Curve b in Fig. 11(a) was measured at a low $\langle \delta V_R \rangle$ value between two peaks; its amplitude is lower than that of curve c, which was taken at a nearby peak position. The shape of the power spectrum at the peak position is very close to that of the $1/f$ noise, while at the bottom position it deviates appreciably from the $1/f$-type distribution, as shown by curve b. Curve a in Fig. 11(a), which was obtained from the first peak (near critical current) position, is an exception: It is close to the Lorentzian-type distribution. For the sake of comparison, the power spectrum at the beginning of the quasilinear region is also shown in Fig. 11(a), as indicated by curve d, which shows the Lorentzian distribution. The $1/f$ noise has long been a puzzling problem in solid-state physics; despite a large number of work done on this subject,[31] a satisfactory general explanation has yet to be found. The $1/f$ noise in our experiments is discussed in Sec. V.

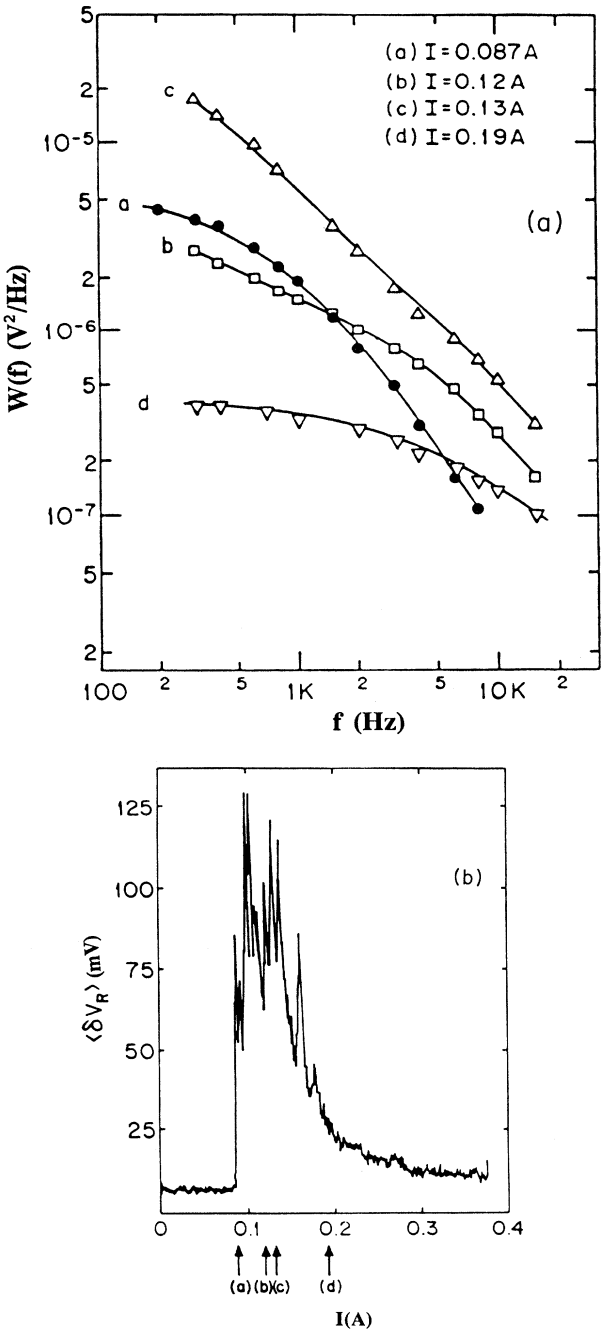

FIG. 11. (a) Series of power spectra taken from sample 4 at $T=4.22$ K and $H=52$ Oe, with the current values shown in the figure and also indicated by arrows in (b). (b) The $\langle \delta V_R \rangle$-vs-$I$ curves corresponding to the power spectra shown in (a) with the specific current values indicated by arrows.

IV. MODEL FOR FLUX-FLOW NOISE IN THE QUASILINEAR REGION

A very important quantity for calculating the noise-power spectrum is the autocorrelation function, which is defined as

$$\psi(t,T)=\langle Y(t)*Y(t+T)\rangle \ , \tag{2}$$

where $Y(t)$ is a physical quantity under consideration. For a statistically stationary system, $\psi(t,T)$ should be independent of t, which means $\psi(t,T)=\psi(T)$. The autocorrelation function is related to the power spectrum $W(f)$ of $Y(t)$ by the Wiener-Khintchine theorem[4]

$$W(f)=4\int_0^\infty \psi(T)\cos(2\pi fT)dT \tag{3}$$

and

$$\psi(T)=\int_0^\infty W(f)\cos(2\pi fT)df \ . \tag{4}$$

In the present experiment, we tried unsuccessfully to explain our results by using the shot-noise model[3] or the modified shot-noise model by Clem.[20] First of all, none of these models relates noise with the Lorentzian spectra. Second, the shot-noise model predicts that the characteristic frequency should decrease as the width of the loop is increased and be independent of the length of the loop; our experimental results give just the opposite, as illustrated in Figs. 8 and 9. These observations are important clues in the construction of our model described in the following.

A schematic diagram representing the experimental arrangement is depicted in Fig. 12 where the dots represent the flux bundles and the rectangle represents the detection loop. The boundary of the sample is not shown in the figure. The direction of the current in the sample is parallel to the long side of the rectangular loop; the flux bundles move in a direction perpendicular to both H and J. If one bundle enters the loop followed by a bundle leaving the loop, a rectangular pulse appears at the output. This forms the basic mechanism for the pulse signals detected in our system.

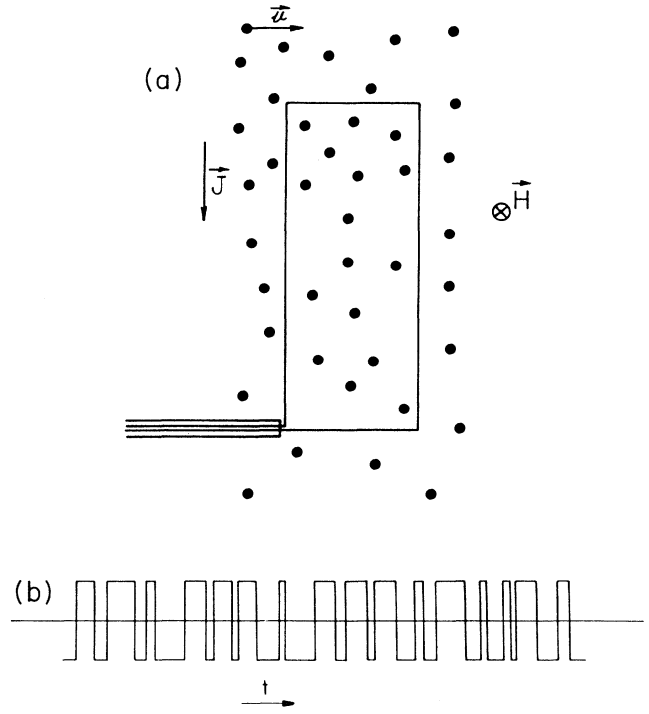

FIG. 12. (a) Schematic representation for flux flow and a detection loop. (b) A schematic representation of an ideal SQUID output voltage as a function of time.

The samples used are polycrystalline alloys of In-Pb with a large number of bulk defects and grain boundaries, as well as surface defects. All of these may act as pinning centers for flux lines. If the current passed through the sample is below the critical current, all the flux lines are pinned by these pinning centers, which may be viewed as potential barriers for the flux lines. The Lorentz force is balanced by the pinning force, although the potential barriers from different kinds of pinning centers are not the same. When the current is increased, flux lines should build up at the pinning centers and form bundles until the Lorentz force plus the forces between flux lines exceed the pinning force. This condition determines the critical current for flux motion or the onset of a voltage in the superconductor. There is no reason to assume that all flux lines depin at the same critical current. In fact, the complex structure in the near-onset region is caused by different kinds of pinning centers giving rise to different current values needed for depinning.

When the current is sufficiently large to bring the system to the quasilinear region where the Lorentz force is much larger than most of the pinning forces, the difference between pinning centers becomes less important. In this region it is reasonable to assume that all the flux bundles have nearly the same velocity. It is also possible that these bundles may be ordered; thus their motion could become correlated.

To calculate the flux-flow noise power, one would necessarily resort to some simplifying approximations. Let us first consider a small detecting loop which only detects a more or less one-dimensional chain of flux bundles. If all the bundles are of the same size, their motion with nearly the same velocity in the same direction will give rise to square-wave pulses in the detector output [see Fig. 12(b)]. It has been tacitly assumed that each entering (leaving) event is followed by a leaving (entering) event; thus the bundles are not totally independent of each other.

This simple model shows that the characteristic frequency of the square-wave output is independent of the detector width W. Since the detector contains many flux bundles, the average duration of the square-wave pulses can be much shorter than the transit time W/v for each individual bundle to cross the detector.

Now let us extend the length L to contain more flux bundles in the detector, as shown in Fig. 12(a), assuming once again that all the bundles are of the same size and move in the same direction with nearly the same velocity. If the sample is homogeneous, it is likely that the probability of two same events (two flux lines both entering or both leaving the detector loop) to follow each other should be smaller than the probability of two different events following each other (i.e., one flux line entering and another one leaving or vice versa). Our assumption that different events are following each other, as in the one-dimensional chain model discussed above, should still be a good approximation. Hence the detector output for the two-dimensional flux flow in the same direction should also exhibit largely square-wave pulses, although the frequency is clearly much higher than that of a single chain. This is in contrast to the case of completely random events where it is well known that the characteristic frequency is independent of the number of occurrences per unit time. The point is due to the fact, as in the present model, that the pulses are not entirely random in relation to one another since a sharp voltage increase must always follow a sharp decrease and vice versa.

For a simple calculation of the noise power, the following assumptions were made: (i) All flux bundles move in the same direction with the same velocity. (ii) The bundles are of the same size. (iii) An entering (leaving) event is followed by a leaving (entering) event. (iv) Any event causes an abrupt jump of $2V_N$ at the rf SQUID output. (v) Successive events (either entering or leaving) are uncorrelated.

Based on the above assumptions, the ideal ac signal at the SQUID output is a sequence of random-width square-wave pulses with amplitude $\pm V_N$. If we assume f_c as the average number of pulses per second, the autocorrelation function can be shown[4] to take the following form:

$$\psi(T)=V_N^2\exp(-f_cT)[1-f_cT+(f_cT)^2/2-\cdots] \\ =V_N^2\exp(-2f_cT)\ . \tag{5}$$

The corresponding noise-power spectrum can be calculated by using the Wiener-Khintchine theorem [Eq. (3)] to yield

$$W(f)=4V_N^2\int_0^\infty \exp(-2f_cT)\cos(2\pi fT)dT$$
$$=(2V_N^2/f_c)[1+(\pi f/f_c)^2]^{-1}\ . \quad (6)$$

There are several features we can see immediately from the structure of the power spectrum. It has a $A[1+(\pi f/f_c)^2]^{-1}$ shape, which is consistent with our experimental data. The characteristic frequency f_c should indicate the average total number of bundles entering (or leaving) the loop per second. The noise power at zero frequency, $W(0)$, is inversely proportional to f_c and proportional to V_N^2. This model not only explains our results in the quasilinear region, but also forms a basis for the explanation of the $1/f$ noise in the near-onset region.

Our model is somewhat similar to the chain model[5] in which the bundles are assumed to move along the same path in a chain across the width W. An increase of L therefore leads to an increase in the characteristic frequency due to the presence of more chains.

V. DISCUSSION

A. Bundle size

One important quantity we would like to obtain from the flux-flow noise measurements is the bundle size Φ. According to our simple model, when a bundle enters the detection loop, it gives rise to a voltage jump of $+2V_N$ at the SQUID output; Φ can then be derived from the noise-power spectrum [Eq. (6)] extrapolated to zero frequency, viz.,

$$W(0)=\text{const}\times\Phi^2/(2f_c)\ . \quad (7)$$

This is also the method used by other investigators to obtain the bundle size.

The variation of $W(0)$ can be compared with power-spectra measurements. Figure 13 shows the power spectra taken from the same sample at two sufficiently large but different current values with otherwise the same conditions. The bundle size does not change significantly in the high-current region. The lower value of $W(0)$ at higher current is mainly due to an increase of f_c.

Because of the way the power-spectrum measurement was made in log scale, $W(0)$ is not sensitive to small changes in the external conditions. Sometimes there was a low-frequency reduction in the power spectrum, which made it difficult to obtain an accurate value of $W(0)$. As a result, it is not very reliable to determine the bundle size from the power-spectrum measurement. According to our model, the peak-to-peak amplitude of the voltage flip in the quasilinear region is proportional to the bundle size; hence a more direct way to obtain the bundle size is to measure the amplitude of the noise directly. In the quasilinear region, the value of $\langle \delta V_R \rangle$ is proportional to the average bundle size; therefore, the real bundle size can be determined after calibrating the response of the detection loop with a known input flux. This is illustrated in Fig. 14, which shows the average bundle size versus the reduced magnetic field with the temperature as a parameter while $J-J_0$ is kept constant. The bundle size is expressed in units of the flux quantum Φ_0 ($=ch/2e$). The lower limit of this measurement is due to the intrinsic noise of the SQUID, which is approximately 16 mV in the present experimental configuration. This number is equal to the response of the SQUID to eight flux quanta. Therefore, only signals greater than eight flux quanta can be determined in our experiments.

The bundling of the flux lines is mainly caused by pinning effects. If the pinning potential barrier is too high for single flux line to overcome, the flux lines may gather as a bundle until they can move over the barrier. The forces driving the bundles against the pinning barrier include the Lorentz force due to the transport current and the repulsive force between the flux lines inside and outside the individual bundle. Both forces increase as the bundle size builds up, until the total force is large enough

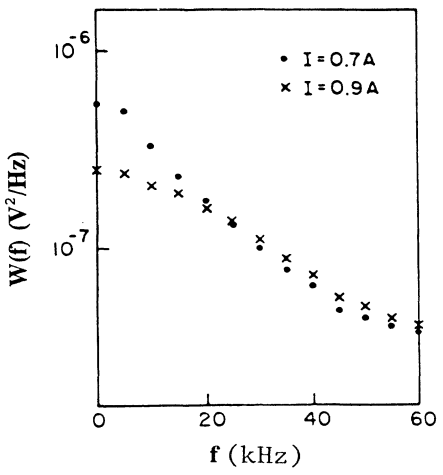

FIG. 13. Power spectra obtained with sample 2 at $T=3.447$ K and $H=227.5$ Oe for two different current values.

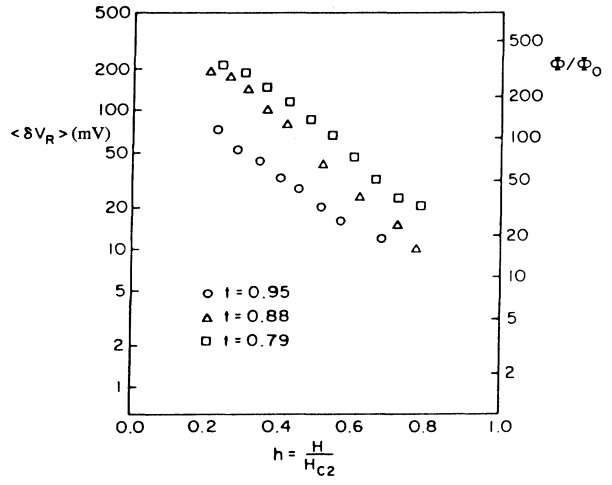

FIG. 14. Average ac voltage $\langle \delta V_R \rangle$ and bundle size vs reduced magnetic field with the temperature as a parameter. Data were taken from sample 6 at $I-I_0=0.25$ A. The bundle size is expressed in units of the magnetic-flux quantum Φ_0.

to move the bundle over the pinning barrier. For a given type of barrier, the minimum bundle size necessary to overcome flux pinning at the onset of flux motion therefore decreases with increasing transport current.

In the quasilinear region, we have found that $\langle \delta V_R \rangle$ decreases monotonically with increasing current. This result suggests that the average bundle size may actually decrease, probably as a result of splitting of large bundles into smaller ones. The decrease in $\langle \delta V_R \rangle$ is slower for high-current values, suggesting that the bundle size will eventually reach a lower limit.

In the near-onset region, since several different kinds of pinning centers are involved, the size of moving bundles can be quite nonuniform; $\langle \delta V_R \rangle$ shows large fluctuations, and therefore it cannot be reliably used to obtain the average bundle size. By detailed examination of oscilloscope traces such as shown in Fig. 3(b), the height of voltage jumps in this region is roughly 3 to 4 times larger than that in the quasilinear region, indicating that the bundle size is also about 3 to 4 times larger than those shown in Fig. 14.

Figure 14 shows that the bundle size decreases as the magnetic field is increased, because an increase in magnetic field represents a decrease of the separation and stronger repulsive force between flux lines; hence this should lead to a decrease of the bundle size. Similarly, the effective pinning barrier decreases as the temperature is raised, also resulting in a decrease of the bundle size, as shown in Fig. 14.

B. Number of observed flux bundles

We have also obtained $N_{\rm obs}$, the number of moving flux bundles from the observed voltage flips per second, and compared it with the total number of flux-line changes in the detection loop per second, $N_{\rm calc}$, calculated from the dc voltage. $N_{\rm obs}$ and $N_{\rm calc}$ can be estimated from

$$N_{\rm obs}=f_c\Phi \tag{8}$$

and

$$N_{\rm calc}=V/\Phi_0 \ . \tag{9}$$

Both quantities are expressed in units of Φ_0. Taking Fig. 5(e) as an example, f_c is equal to 16.7 kHz, the flux bundle size is equal to $98\Phi_0$, V is equal to 33 μV, and the length of the detection loop is equal to half of the distance between the voltage leads; hence $N_{\rm obs}=1.64\times10^6$ flux quanta per second and $N_{\rm calc}=8.0\times10^9$ flux quanta per second.

These results show that only a small fraction of the total moving flux lines contribute to the observed noise. This suggests that when the flux lines are set in motion, only a small fraction of the flux lines form bundles large enough to be detected by the present SQUID detector. Other flux lines either move in the single-flux quantum state or in small bundles which cannot be detected by the present setup. This result is also consistent with the picture given by Dirks and Heiden.[14]

C. Peaks in $\langle \delta V_R \rangle$ and $1/f$ noise

The most striking feature of the $\langle \delta V_R \rangle$-versus-$I$ curve is the structure of peaks in the near-onset region. The repeatable feature of these peaks reveals some intrinsic properties of the superconductor. We have found that the $1/f$ noise is also related to these peaks.

In each superconductor sample, different kinds of pinning centers appear as different potential barriers to the flux lines. The depinning energies for different pinning centers are not the same. In our system there are several kinds of pinning centers which may include bulk defects, grain boundaries, and surface defects. Any specific sharp jump in the $\langle \delta V_R \rangle$-versus-$I$ curve indicates that some flux bundles start to depin from one kind of pinning center, and the current at this point represents the apparent subcritical current for this particular kind of pinning. The density and strength of pinning centers are strongly dependent on the morphology and metallurgical conditions of the sample; hence the detailed fine structures of this curve are not the same for different samples. Nevertheless, the general feature is always similar for all the samples investigated.

In the near-onset region, because the critical currents for various pinning centers are not the same, the effective forces on flux bundles at different pinning centers could be quite different, and the velocities for different bundles should also be different, especially at the $\langle \delta V_R \rangle$ peak positions. When some bundles just start to move, the velocity of these bundles could be very low, while other moving bundles may have already acquired high velocities. The assumptions in the model used to explain the quasilinear region therefore become invalid in the near-onset region. The probability for two or more voltage-jump events of the same kind to follow each other may become large, or even dominant. The amplitude of the signal arising from these successive events of the same kind can be several times larger than that caused by a single voltage jump. In Fig. 3(b) this kind of overlap is clearly visible; this gives rise to the large amplitudes of voltage fluctuations at the subcritical-current positions.

The $1/f$ noise is also related to the spread of velocities of the moving flux bundles. According to the model developed for the quasilinear region, the power spectrum should be Lorentzian for a specific subgroup of bundles of the same size and with the same velocity, i.e.,

$$w(f)=(\Phi^2\tau/2)[1+(\pi f\tau)^2]^{-1} \ , \tag{10}$$

where $\tau=1/f_c$. The total-power spectrum generated by all the bundles can be obtained by integrating Eq. (10) over a distribution of τ to yield

$$W(f)=\int w(f)g(\tau)d\tau \ , \tag{11}$$

where $g(\tau)$ is a distribution function for τ. The actual distribution function is dependent on the structure of pinning centers and very sensitive to the current value. In order to fit the $1/f$ noise obtained in the near-onset region, the method first used by van der Ziel[32] for analyzing the noise in semiconductors is employed. We assume the simplest possible form for $g(\tau)$, namely,

$$g(\tau)=\begin{cases} A/\tau\ , & \tau_1\le\tau\le\tau_2 \\ 0\ , & \text{otherwise}\ , \end{cases} \tag{12}$$

where A is a normalization constant. Integrating Eq. (11) with the above form for $g(\tau)$, we obtain

$$W(f)=(A\Phi^2/2\pi f)[\arctan(\pi f\tau_2)-\arctan(\pi f\tau_1)]\ . \tag{13}$$

By adequately choosing τ_1 and τ_2, we can reproduce the $1/f$ shape of $W(f)$ in the frequency region of interest.

We note that the data points sometimes show small deviations in the middle of the $1/f$-noise curve, as can be seen from curves *a*, *b*, and *d* in Fig. 10. The reason for this deviation can be explained by a modified distribution function. A possible distribution to account for this deviation is to define $g(\tau)$ in two separate τ domains. This distribution seems very plausible from physical consideration. When the system is near or at a $\langle\delta V_R\rangle$ peak position, there are certain bundles already in motion with sufficiently high velocity, while some other bundles just start to move with low velocity. Because the lack of bundles moving with velocities between these high and low values, a deviation can appear in the middle of the power spectrum. The data can be fitted by assuming

$$g(\tau)=\begin{cases} A/\tau\ , & \tau_1\le\tau\le\tau_2 \text{ and } \tau_3\le\tau\le\tau_4 \\ 0\ , & \text{otherwise}\ . \end{cases} \tag{14}$$

As an example, the data of curve *a* in Fig. 10 were fitted this way. The result is shown in Fig. 15. Dots are data points, and the solid curve is obtained with $\tau_1=5\times10^{-5}$ sec, $\tau_2=8\times10^{-5}$ sec, $\tau_3=6\times10^{-4}$ sec, and $\tau_4=4\times10^{-3}$ sec, respectively. The deviation structure in the middle of the curve is reproduced. The value for $f=2/(\tau_1+\tau_2)$, which corresponds to the high-speed group, is approximately 15 kHz. This value is consistent with the data obtained in the quasilinear region. The good fit supports our assertion that the distribution function for two separate groups of flux bundles can account for the deviations in the $1/f$ noise.

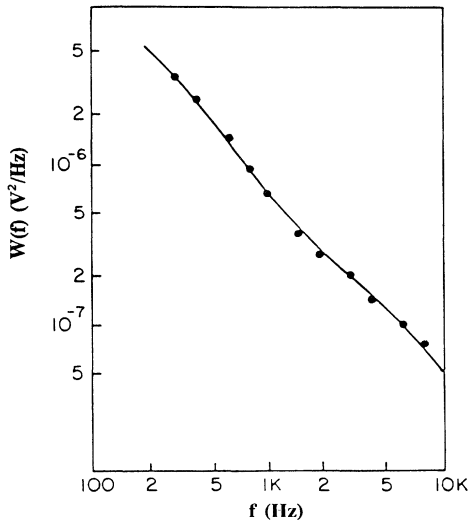

FIG. 15. Results of fitting the data points of curve *a* in Fig. 10. The dots are experimental data. See text for details.

When some flux lines move faster than the others, there should be a drag force between them. This interaction causes the difference between the velocities of different groups of bundles to decrease very rapidly as the current is increased away from the peak position; this results in the fast decrease of the amplitude of $\langle\delta V_R\rangle$. It also leads to a deviation from the $1/f$-type noise-power spectrum at the minima positions in the $\langle\delta V_R\rangle$-versus-I curves. It should be remarked that according to the model developed above, the velocities of all moving bundles are low at the onset of $\langle\delta V_R\rangle$, the spread of velocities is small, and the power spectrum should be more like the Lorentzian shape. This is borne out in our experiment, as shown by curve *a* in Fig. 11(a).

In the near-onset region, the bundle sizes are different too. This will also contribute to the deviation from the Lorentzian type of power spectrum. But in light of the analysis presented above as well as the good fits of experimental data, we believe the spread of velocities is the main cause for the occurrence of the $1/f$ noise in the present experiment.

D. Flicker noise

Because the SQUID we used can only be operated at temperatures higher than 2.9 K, all of our measurements were performed above the λ point of liquid helium. The flicker noise first studied by van Gurp[3] was observed at relatively high currents. When the SQUID output was monitored by an oscilloscope, it was very easy to identify it. At first, it appeared as an isolated slow variation superimposed on the high-frequency flux-flow noise. The frequency of the flicker noise could be as low as 0.1 Hz. At this point the dissipation per unit area was approximately 0.6 mW/cm^2. As the current was increased, both the frequency and amplitude of the flicker noise increase. Figure 16 is a picture of the flicker noise taken from an oscilloscope. The current value at which the flicker noise started to appear always falls into the quasilinear region. The noise in the near-onset region does not include any

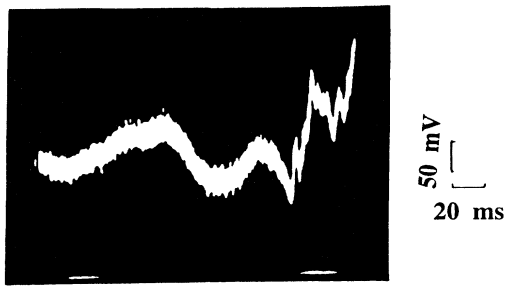

FIG. 16. Picture of flicker noise obtained with sample 2 at $T=3.447$ K, $H=260$ Oe, $I=0.8$ A, and $V=785$ μV. The power dissipation per unit area under these conditions is 4 mW/cm^2.

flicker noise. The frequency of the flicker noise (about 10 Hz or lower) is much lower than that of the flux-flow noise (a few kHz or higher); hence these two types of noise could be easily separated in the power spectrum. In the high-current regime, there was a sharp increase in the very-low-frequency portion of the power spectrum, which was due to the flicker noise; this was discarded in our data analysis.

VI. CONCLUSIONS

We have measured the flux-flow noise in type-II superconductors by using a rf SQUID. Results show that the behavior of flux flow in the quasilinear region is quite different from that in the near-onset region.

A model was developed to explain the data for the quasilinear region. A noise-power spectrum of the Lorentzian type was obtained from the model and found to be in agreement with our measurements. A numerical estimate of the number of flux quanta, N, detected per second was made by using the characteristic frequency f_c and the time-averaged dc voltage V. The low value of N suggests that only a small fraction of moving flux lines form large bundles (greater than $8\Phi_0$); the other flux lines either move in smaller bundles or in a single-flux quantum state. This result supports the picture given by Dirks and Heiden.[14] According to our model, the bundle size is proportional to the amplitude of the noise signal in the quasilinear region, and this can be obtained directly by measuring the ac amplitude of the SQUID output. Our present detector is only sensitive to flux bundles greater than $8\Phi_0$; by a modified design, this sensitivity can be improved to detect effects arising from a single moving flux quantum.

In the near-onset region, because different kinds of pinning centers have different depinning energies, the $\langle \delta V_R \rangle$-versus-$I$ curves show several distinct peaks. Each peak position represents the apparent critical current for a specific kind of pinning center. This experiment shows that the SQUID measurement also gives information about the effects of pinning centers. The power spectra with current biased at the $\langle \delta V_R \rangle$ peak positions show $1/f$ noise, which is quite different from the power spectrum in the quasilinear region. The $1/f$-type noise spectrum was well fitted by using a model in which the velocities of flux bundles are assumed to spread over different ranges. The reason for this velocity spreading is due to different depinning energies associated with different kinds of pinning.

Our experiment shows that the noise-power spectrum can change from $1/f$ type to Lorentzian type, or vice versa, by varying the bias current. Measurements of the flux-flow noise in superconductors not only reveal useful information on the dynamical properties of flux motion, but also provide a convenient way to investigate the $1/f$ noise and its variations.

The technique and experimental results described in the present paper are also applicable to the study of high-T_c superconductors. The effects of flux pinning and weak links are very important in controlling the critical-current density in the high-T_c materials. In particular, the grain boundaries could play a dual role of forming the weak links as well as pinning centers. It should be of both fundamental and technical interest to find a correlation between the critical-current density of the superconductors and the dynamical state of flux flow. The greatly improved sensitivity of detecting the onset of flux flow by our "flux-counting method" over the usual I-V curve measurement, as well as the noise spectrum and ac response of the system, should provide a useful means for understanding the flux dynamics of the high-T_c superconductors. This work is now in progress.

[1] R. P. Huebener, *Magnetic Flux Structures in Superconductors* (Springer-Verlag, Berlin, 1979).

[2] For a review, see J. R. Clem, Phys. Rep. **75**, 1 (1981).

[3] D. J. van Ooijen and G. J. van Gurp. Phys. Lett. **17**, 230 (1965); G. J. van Gurp, Phys. Rev. **166**, 436 (1968).

[4] D. K. C. MacDonald, *Noise and Fluctuations: An Introduction* (Wiley, New York, 1962)

[5] F. Chilton, in *Proceedings of the Conference on Fluctuations in Superconductors,* edited by W. S. Goree and F. Chilton (Stanford Research Institute, Menlo Park, CA, 1968), p. 193.

[6] J. M. A. Wade, Philos. Mag. **23**, 1039 (1971).

[7] P. Jarvis and J. G. Park, J. Phys. F **4**, 1238 (1974).

[8] P. Jarvis and J. G. Park, J. Phys. F **5**, 1573 (1975).

[9] F. Habbal and W. C. H. Joiner, J. Low Temp. Phys. **28**, 83 (1977); F. Habbal and W. C. H. Joiner, Phys. Lett. **60A**, 434 (1977).

[10] J. Thompson and W. C. H. Joiner, Phys. Rev. B **20**, 91 (1979).

[11] J. B. Kruger and C. Heiden, in *Low Temperature Physics LT 12,* edited by E. Kanda (Academic, Tokyo, 1971), p. 415.

[12] C. Heiden and H. P. Friedrich, Solid State Commun. **9**, 323 (1971).

[13] C. Heiden, Solid State Commun. **18**, 253 (1976).

[14] H. Dirks and C. Heiden, in *Noise in Physical Systems,* Proceedings of the Fifth International Conference on Noise, edited by D. Wolf (Springer-Verlag, Berlin, 1978), p. 229.

[15] K. Beckstette and C. Heiden, in *Noise in Physical Systems* (Ref. 14), p. 234.

[16] C. Heiden, D. Kohake, W. Krings, and L. Rathe, J. Low Temp. Phys. **27**, 1 (1977).

[17] D. Kohake and C. Heiden, J. Low Temp. Phys. **40**, 531 (1980).

[18] B. Müller, C. Heiden, P. S. Li, and J. R. Clem, J. Low Temp. Phys. **43**, 165 (1981).

[19] R. E. Burgess, Physica (Utrecht) **55**, 369 (1971).

[20] J. R. Clem, Phys. Rev. B **1**, 2140 (1970).

[21] J. R. Clem, J. Phys. (Paris) Colloq. **39**, C6-619 (1978).

[22] J. R. Clem, in *Noise in Physical Systems,* (Ref. 14), p. 214.

[23] J. R. Clem, J. Low Temp. Phys. **42**, 363 (1981).

[24] A. van der Ziel, Phys. Lett. **25A**, 672 (1967).

[25] S. W. Shen, Appl. Phys. Lett. **17**, 415 (1970).

[26] S. W. Shen and A. van der Ziel, Physica (Utrecht) **64**, 587 (1973).

[27] H. M. Choe and A. van der Ziel, Physica (Utrecht) B **81**, 237 (1976).

[28] W. J. Yeh and Y. H. Kao, Phys. Rev. Lett. **53**, 1590 (1984).

[29] M. J. Ferrari, M. Johnson, F. C. Wellstood, J. Clarke, P. A. Rosenthal, R. H. Hammond, and M. R. Beasley, Appl. Phys.

Lett. **53**, 695 (1988); M. J. Ferrari, M. Johnson, F. C. Wellstood, J. Clarke, D. Mitzi, P. A. Rosenthal, C. B. Eom, T. H. Geballe, A. Kapitulnik, and M. R. Beasley, Phys. Rev. Lett. **64**, 72 (1990).

[30]B. Byrnak and F. B. Rasmussen, in *Proceedings of the International Conference on the Science of Superconductivity,* edited by F. Chilton (North-Holland, Amsterdam, 1971), p. 357.

[31]For a review, see P. Dutta and P. M. Horn, Rev. Mod. Phys. **53**, 497 (1981).

[32]A. van der Ziel, Physica **16**, 359 (1950).